Spontaneous Anomalous Hall Effect Arising from an Unconventional Compensated Magnetic Phase in a Semiconductor

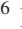R. D. Gonzalez Betancourt[1,2,3] J. Zubáč[2,4] R. Gonzalez-Hernandez,[5,*] K. Geishendorf,[2] Z. Šobáň,[2]
G. Springholz,[6] K. Olejník,[2] L. Šmejkal,[7,2] J. Sinova,[7,2] T. Jungwirth,[2,8] S. T. B. Goennenwein,[9,1]
A. Thomas,[1,3] H. Reichlová,[1] J. Železný,[2] and D. Kriegner[1,2,†]

[1]*Institute of Solid State and Materials Physics, Technical University Dresden, 01062 Dresden, Germany*
[2]*Institute of Physics, Academy of Sciences of the Czech Republic, Cukrovarnická 10, 162 00 Praha 6, Czech Republic*
[3]*Leibniz Institute of Solid State and Materials Research (IFW Dresden), Helmholtzstr. 20, 01069 Dresden, Germany*
[4]*Charles University, Faculty of Mathematics and Physics, Ke Karlovu 3, 121 16 Prague 2, Czech Republic*
[5]*Departamento de Fisica y Geociencias, Universidad del Norte, Barranquilla 080020, Colombia*
[6]*Institute of Semiconductor and Solid State Physics, Johannes Kepler University Linz, Altenbergerstr. 69, 4040 Linz, Austria*
[7]*Institut für Physik, Johannes Gutenberg Universität Mainz, 55128 Mainz, Germany*
[8]*School of Physics and Astronomy, University of Nottingham, Nottingham NG7 2RD, United Kingdom*
[9]*Department of Physics, University of Konstanz, 78457 Konstanz, Germany*

The anomalous Hall effect, commonly observed in metallic magnets, has been established to originate from the time-reversal symmetry breaking by an internal macroscopic magnetization in ferromagnets or by a noncollinear magnetic order. Here we observe a spontaneous anomalous Hall signal in the absence of an external magnetic field in an epitaxial film of MnTe, which is a semiconductor with a collinear antiparallel magnetic ordering of Mn moments and a vanishing net magnetization. The anomalous Hall effect arises from an unconventional phase with strong time-reversal symmetry breaking and alternating spin polarization in real-space crystal structure and momentum-space electronic structure. The anisotropic crystal environment of magnetic Mn atoms due to the nonmagnetic Te atoms is essential for establishing the unconventional phase and generating the anomalous Hall effect.

The ordinary and anomalous Hall effects are prominent phenomena in condensed matter physics and spintronics that refer to a nondissipative current, $\mathbf{j}_H = \mathbf{h} \times \mathbf{E}$, generated in a transverse direction to the applied electric field $\mathbf{E}$ [1,2]. The corresponding antisymmetric transverse components of the conductivity tensor, $\sigma_{ij}^a = -\sigma_{ji}^a$, form a pseudovector $\mathbf{h} = (-\sigma_{yz}^a, \sigma_{xz}^a, -\sigma_{xy}^a)$ whose components flip sign under the time-reversal transformation $(\mathcal{T})$ [1,2]. In the ordinary Hall effect, $\mathbf{h}$ is typically proportional to an applied external magnetic field that breaks the $\mathcal{T}$ symmetry and couples to the electronic degrees of freedom via the Lorentz force. In contrast, the anomalous Hall effect (AHE) reflects the $\mathcal{T}$-symmetry breaking in the crystal and electronic structure associated with an internal magnetic order in a material [1,2]. The AHE can, therefore, generate a spontaneous Hall signal even in the absence of an external magnetic field. It is established that the AHE can arise from a macroscopic magnetization in ferromagnets, or a noncollinear order of spins on certain lattices of magnetic atoms [1,2].

Following a prediction for RuO_2 [3], the research of the AHE has recently turned to materials belonging to the abundant family of crystals with compensated collinear antiparallel ordering of spins [3–7], for which the AHE and other $\mathcal{T}$-symmetry breaking spintronic phenomena have been traditionally considered to be excluded due to the vanishing net magnetization [2]. The surprising emergence of the $\mathcal{T}$-symmetry breaking responses in these compensated magnetic crystals has been recently ascribed to an unconventional magnetic phase [7,8]. It is characterized by an alternating spin polarization in both real-space crystal structure and momentum-space electronic structure, which has suggested to term this unconventional phase altermagnetism [7,8]. Crystals hosting altermagnetism have the opposite-spin sublattices connected by crystal rotation transformations (proper or improper and symmorphic or nonsymmorphic). In contrast, conventional antiferromagnets are characterized by the translation or inversion symmetry connecting the opposite-spin sublattices [9,10]. A systematic symmetry based classification and description of this unconventional magnetic phase has been developed using a nonrelativistic spin-group formalism [7,8].

RuO_2 is a prominent member of the altermagnetic family because of its metallic conduction combined with magnetic ordering above room temperature [11,12], and because of the presence of the AHE [3,13] and of nonrelativistic spin splitting, charge-spin conversion, and giant magnetoresistive phenomena [3,13–21]. Moreover, RuO_2

is a representative of the specific subclass of altermagnets in which an anisotropic arrangement of nonmagnetic atoms in the crystal (O atoms in RuO_2) breaks the inversion and translation symmetry, while preserving the rotation symmetry, connecting the opposite-spin sublattices. Because of the essential role of nonmagnetic atoms, the AHE in materials like RuO_2 has been referred to as originating from a crystal $\mathcal{T}$-symmetry breaking mechanism [3,4,6].

Transport measurements in RuO_2 have confirmed the presence of the AHE signals [13]. However, the experiments relied on an externally applied magnetic field that served as a tool for reorienting the magnetic order vector from the [001] easy axis. Incidentally, this magnetic easy axis is a singular direction of the magnetic order vector in RuO_2 for which the AHE vanishes by symmetry [3,13].

In this Letter we report the experimental observation of the AHE in thin-film α-MnTe with a room temperature compensated collinear magnetic order [22]. Despite the extensive exploration of MnTe in the past [22–34], the AHE has not been theoretically or experimentally identified in this material prior to our Letter. We highlight that the MnTe structure shares with RuO_2 the essential role of nonmagnetic atoms (Te atoms in case of MnTe) in the formation of the altermagnetic phase, and the corresponding $\mathcal{T}$-symmetry breaking phenomena, including the AHE. In contrast to RuO_2, our measurements in MnTe show hysteresis and spontaneous AHE signals at zero magnetic field. By symmetry analysis and density functional theory (DFT) calculations we show that the spontaneous nature of the AHE results from the favorable magnetic easy axes in our MnTe thin film.

The other major distinction of MnTe from metallic RuO_2 and common ferromagnets or noncollinear magnets with metallic conduction is that stoichiometric MnTe is an intrinsic room-temperature magnetic semiconductor [22,24,26,35,36]. The prospect of integrating $\mathcal{T}$-symmetry breaking spintronic phenomena with field-effect transistor functionalities in one material has driven the research of ferromagnetic semiconductors for decades, in particular of the III–V compounds that become ferromagnetic when heavily doped with Mn [37–39]. However, the required heavy charge dopings compromise the semiconducting nature of the host compounds, while the ferromagnetic transition temperatures have remained well below room temperature, i.e., far below the Curie temperatures of common transition-metal ferromagnets. Our observation of the AHE in MnTe demonstrates that altermagnetism can remove the roadblock associated with the notorious incompatibility of robust high-temperature ferromagnetism with semiconducting (insulating) band structures.

A schematic crystal of α-MnTe with NiAs structure (crystallographic space group $P6_3/mmc$ #194 [40]) is shown in Fig. 1(a). The magnetic moments on Mn have a parallel alignment within the c planes and an antiparallel alignment between the planes which avoids frustration in
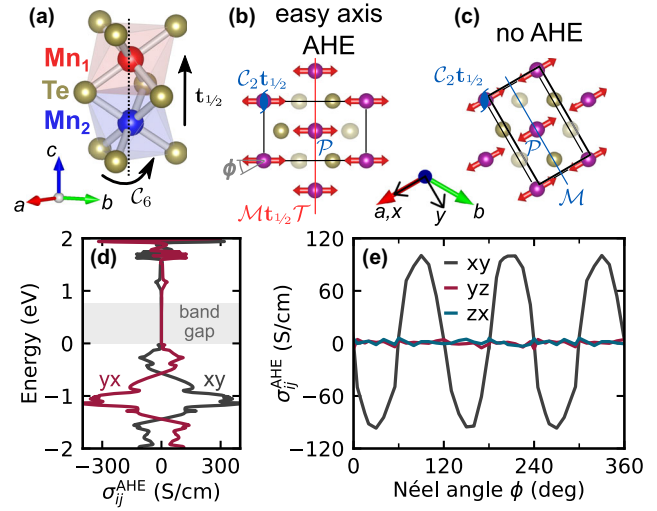

FIG. 1. Theoretical calculation of spontaneous anomalous Hall signal in collinear MnTe: (a) Atomic configuration of Mn (blue or red) and Te (gold) with hexagonal NiAs structure. The two magnetic sublattices are connected by a sixfold screw axis along [0001]. (b) and (c) Magnetic moment configurations of the hexagonal c planes with magnetic moments (red arrows) oriented along $[1\bar{1}00]$ and $[2\bar{1}\,\bar{1}\,0]$, respectively. The magnetic unit cell shape (black line) and crystal symmetry operations corresponding to the generators of the magnetic point groups are indicated in the panels. Te atoms at different heights are indicated by different color saturation. (d) DFT Anomalous Hall conductivity vs. Fermi energy calculated for the moment configuration of panel (b) and Hall current along x direction. (e) Transverse conductivity components for the Fermi energy 0.25 eV below the valence band maximum as a function of the Néel vector orientation. The angle ϕ is defined with respect to the a axis.

the magnetic order. The crystallographic translation or inversion transformations do not connect the opposite spin sublattices because of the nonmagnetic Te atoms that occupy noncentrosymmetric positions and form octahedra around the Mn atoms. This symmetry-lowering arrangement of nonmagnetic atoms around the magnetic atoms is reminiscent of RuO_2 [3]. The specific realization is, however, different. In RuO_2, the O octahedra belonging to the opposite-spin sublattices share an edge and the two sublattices are connected by a crystallographic nonsymmorphic fourfold rotation C_4 combined with half unit-cell translation. In MnTe, the two opposite-spin sublattices are connected by a nonsymmorphic sixfold rotation C_6 combined with half-unit cell translation along the c axis $\mathbf{t}_{1/2}$ (screw axis), as highlighted by the blue and red shaded face sharing octahedra in Fig. 1(a) [2,41].

The strong nonrelativistic $\mathcal{T}$-symmetry breaking and alternating spin-splitting in the band structure of MnTe, accompanied by zero nonrelativistic net magnetization, is described by a spin Laue group $^26/^2m^2m^1m$ of symmetry transformations in decoupled real and spin space [7]. The spin-group symmetries imply the presence of four spin-degenerate nodal planes crossing the $\mathbf{\Gamma}$-point of the

momentum-dependent electronic structure (*g*-wave symmetry), corresponding to four mirror-symmetry planes combined with spin-space rotation of the compensated collinear spin arrangement on the real-space MnTe crystal [7].

Besides the $\mathcal{T}$-symmetry breaking, additional symmetry-lowering requirements have to be fulfilled by the magnetic state of the crystal to allow for an Hall pseudo-vector **h** [2]. These requirements are described within the formalism of relativistic magnetic-group symmetries in coupled real and spin space because, in general, the AHE in collinear (coplanar) magnets is observed in the presence of spin-orbit coupling [2]. Whether or not the AHE is allowed by the relativistic magnetic symmetries then depends on the orientation of the magnetic-order (Néel) vector with respect to the crystal axes.

Figures 1(b) and 1(c) show two representative orientations of the Néel vector within the *c* plane of MnTe. The first orientation is along the $[1\bar{1}00]$ magnetic easy axis in our thin film [41], which is rotated by $\phi = 30°$ from the crystallographic *a* axis [31,50]. In this case, the generators of the relativistic magnetic point-group $m'm'm$ are the inversion $\mathcal{P}$, a twofold rotation C_2 around the *c* axis, and a mirror perpendicular to the Néel vector combined with time-reversal $\mathcal{MT}$ [indicated in Fig. 1(b)]. This is compatible with the presence of the AHE pseudovector along the *c* axis [2,3,41] and therefore enables the detection of a hysteretic AHE signal. In contrast, for the Néel vector along the *a* axis ($[2\bar{1}\,\bar{1}0]$), the generators of the relativistic magnetic point group mmm are inversion $\mathcal{P}$, the twofold rotation C_2 around *c*, and a mirror $\mathcal{M}$ perpendicular to the Néel vector, which excludes the AHE by symmetry [41].

To calculate the intrinsic Berry-curvature anomalous Hall conductivity (AHC) [1,2], we use the maximally localized Wannier functions based on the DFT framework [41]. The obtained AHC for various Néel vector orientations within the *c* plane corroborate our symmetry analysis. For the Néel vector aligned with the easy axis and current along the *a* axis, the dependence of the AHC on the Fermi energy is shown in Fig. 1(d). AHC values above 300 S/cm are found for states deep in the valance band, while the magnitude diminishes when the Fermi level approaches the valance band edge. Note that for the indices of the components of the AHE pseudovector $\mathbf{h} = (-\sigma_{yz}^{\text{AHE}}, \sigma_{xz}^{\text{AHE}}, -\sigma_{xy}^{\text{AHE}})$, we use a notation in which *x* corresponds to the crystal *a* axis ($[2\bar{1}\,\bar{1}0]$), *y* to the $[01\bar{1}0]$ crystal axis, and *z* to the *c* axis ($[0001]$) of MnTe.

Figure 1(e) shows the AHC components σ_{ij}^{AHE} calculated for a fixed Fermi energy as a function of the Néel vector angle ϕ in the *c* plane measured from the *a* axis. Here *i* labels the Hall current direction and *j* the applied electric-field direction. As expected from symmetry, σ_{xy}^{AHE} is the only nonzero component of the AHE pseudovector, i.e., **h** is parallel to the *c* axis and orthogonal to the in-plane Néel vector. This is strikingly distinct from the conventional AHE in ferromagnets where the Hall vector typically
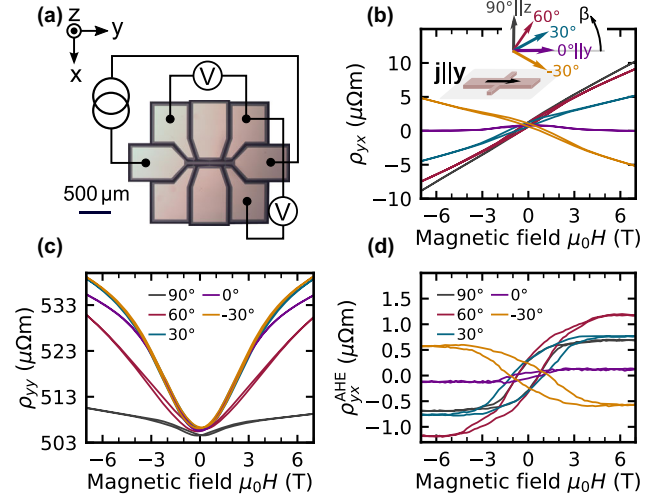

FIG. 2. Magnetic field sweep measurements and AHE at $T = 150$ K. (a) Microscopy image of the Hall bar together with electrical schematics of our measurement. For all transport measurements a moderate current density $j \sim 8 \times 10^6$ A/m² was used. (b) and (c) Transverse and longitudinal resistivities measured during magnetic field sweeps in a geometry indicated by the sketch in (b). (d) Inferred anomalous Hall resistivity given by $\rho_{yx}^{\text{AHE}} \equiv \rho_{yx} - \rho_{yx}^{\text{OHE}} - \rho_{yx}^{\text{even}}$ (see text).

aligns with the magnetization order vector [1]. Similarly, it is distinct from the experimentally observed anomalous Hall effect in RuO₂, ascribed to the Néel vector component parallel to the Hall vector [13]. The symmetry restrictions of MnTe also force $\sigma_{xy}^{\text{AHE}}(\phi)$ to zero every 60°, when the Néel vector is aligned along the *a* axis or equivalent axes in the *c* plane.

For the AHE measurements, we have prepared epitaxial thin films of α-MnTe by molecular beam epitaxy on a single-crystal InP(111)A substrate at a substrate temperature of 380 °C using Mn and Te beam flux sources. Reflection high energy electron diffraction and x-ray diffraction data indicate two-dimensional layer-by-layer growth, high crystallographic quality, and film thickness of 48 nm [41]. For the growth on InP(111)A, the epitaxial relationship is $(0001)[1\bar{1}00]_{\text{MnTe}}\|(111)[11\bar{2}]_{\text{InP}}$, which allows us to perform the desired AHE transport measurements in the *c*-plane. Charge transport in our thin films is enabled by unintentional *p*-type doping commonly observed in MnTe [36,51]. Details of the growth, transmission electron microscopy, and neutron diffraction studies of our films are described by Kriegner and co-workers [22,31].

Hall bar microdevices, shown in Fig. 2(a), were fabricated using electron beam lithography, argon milling, and Cr/Au contacts produced by a lift-off process. The Hall bar is along the *y* axis ($[01\bar{1}0]$), and the magnetic field is applied in the $[01\bar{1}0] - [0001]$ plane at an angle β measured from the Hall-bar direction. In our semiconducting MnTe, the transverse resistivity plotted in Fig. 2(b) is dominated

by the ordinary Hall contribution that is a linear function of the out-of-plane ([0001]) component of the applied magnetic field. The hole concentration and mobility inferred from the measurements in Fig. 2 by assuming a single band picture are 4.9×10^{18} cm^{-3} and 29 cm^2/Vs, consistent with the semiconducting character of MnTe and with a Fermi level within $\sim$20 meV from the valance band edge.

Besides the dominant ordinary Hall signal, the transverse resistivity in Fig. 2(b) contains an anomalous contribution, as seen from the hysteresis with different zero-field spontaneous Hall signals for the opposite field-sweep directions. In contrast, such a hysteretic behavior is absent in the longitudinal resistivity measurement, as shown in Fig. 2(c). The anomalous Hall signal ρ_{yx}^{AHE} is highlighted in Fig. 2(d) where we subtracted the ordinary Hall contribution (ρ_{yx}^{OHE}) from the measured transverse resistivity, and where we also removed the even-in-field contribution defined as $\rho_{yx}^{\mathrm{even}} = [\langle\rho_{yx}(H)\rangle + \langle\rho_{yx}(-H)\rangle]/2$. Here $\langle\rho_{yx}(H)\rangle = [\rho_{yx}(H_{\uparrow}) + \rho_{yx}(H_{\downarrow})]/2$, and $H_{\uparrow(\downarrow)}$ refers to the measurement at the negative-to-positive (positive-to-negative) field sweep [41].

The hysteresis and the opposite zero-field spontaneous Hall signals for opposite field-sweep directions are well pronounced in ρ_{yx}^{AHE} when the applied magnetic field contains an out-of-plane component. This is again explained by symmetry. MnTe can have a weak relativistic magnetization due to terms in the thermodynamic potential that couple the weak magnetization to the Néel vector [52]. The allowed presence of the weak magnetization in zero magnetic field requires in our MnTe the same symmetry lowering as the spontaneous AHE because both effects are described by a pseudovector that is odd under $\mathcal{T}$ [2]. For the Néel vector in the c plane of MnTe, the anomalous Hall and the weak magnetization pseudovectors align with the c axis. Except when the Néel vector is parallel to the a axis or the other equivalent axes for which both effects vanish by symmetry. When an applied out-of-plane magnetic field reverses the weak magnetization, symmetry implies that the Néel vector is also forced via the coupling in the thermodynamic potential to reverse, which results in the flip of the sign of the AHE.

The presence of the in-plane component of the magnetic field in our measurements is favorable for maximizing the observed ρ_{yx}^{AHE} because of the repopulation of domains with the Néel vectors aligned with the three equivalent zero-field easy axes. The repopulation, i.e., the in-plane Néel vector reorientation occurs for in-plane fields above the spin-flop transition which is around 2 T [41]. As a result, the measured AHE at saturation is maximized for $\beta = 60°$, while $\beta = 90°$ gives the lowest saturation field [see Fig. 2(d)].

Note that the decisive role of the out-of-plane field component for determining the sign of the spontaneous and saturated AHE signal is particularly visible for ρ_{yx}^{AHE} traces recorded at $\beta = \pm30°$. While the in-plane component of the field is the same in both of these field-sweep traces, the
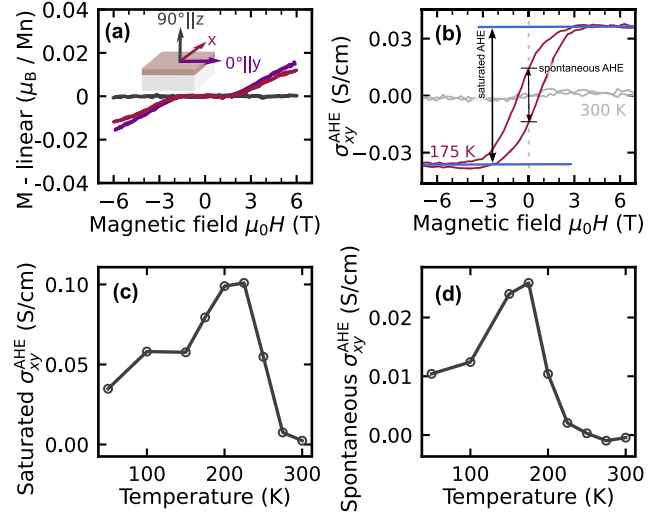

FIG. 3. (a) SQUID magnetization obtained for in-plane and out-of-plane magnetic field measured at 10 K on a 2000 nm thick film. To highlight the absence of remanent magnetization a linear slope obtained in vicinity of zero magnetic field was subtracted from each dataset. Note that the slope contains the susceptibility of MnTe as well as the diamagnetic substrate. (b) AHE conductivity $\sigma_{xy}^{\mathrm{AHE}}$ obtained from the measured ρ_{yx}^{AHE} at 175 and 300 K, and $\beta = 30°$. (c) and (d) Temperature dependence of the spontaneous zero-field and saturated AHE conductivity.

out-of-plane components have the opposite sign and, correspondingly, the measured hysteretic ρ_{yx}^{AHE} also flips sign between the two traces. When removing the magnetic field, some domain randomization occurs due to magneto-striction [22]. This causes a reduction of the spontaneous zero-field AHE signal as compared to the saturated value [Fig. 2(d)].

We also point out that while the weak magnetization facilitates the reversal of the sign of ρ_{yx}^{AHE} by the out-of-plane component of the applied magnetic field, the AHE is not a consequence of the weak magnetization, as discussed in detail by Šmejkal and co-workers [2,3]. The principle origin of the AHE is the $\mathcal{T}$-symmetry breaking due to the compensated antiparallel magnetic order on Mn atoms and the anisotropic crystal environment due to the Te atoms. The relativistic spin-orbit interaction then couples this strong $\mathcal{T}$-symmetry breaking to the charge Hall transport and, analogous but not as a consequence of the other, can also generate the weak magnetization [2,3].

Measurements of the magnetization, shown in Fig. 3(a), are consistent with the above origin of the spontaneous AHE in MnTe, and contrast with the conventional magnetization-induced AHE in ferromagnets. We performed the magnetization measurements using the superconducting quantum interference device (SQUID) technique. The raw SQUID signal is dominated by the diamagnetic contribution from the substrate. After subtracting a linear background, we observe that the remanent out-of-plane magnetization, albeit allowed by symmetry and estimated

to be $\lesssim 2 \times 10^{-4}\ \mu_B/$Mn from first principle calculations, is unobservable even within the high-resolution of the employed SQUID technique. This contrasts with the clearly observable spontaneous zero-field signals and hysteresis in the AHE measurements. Note that for in-plane magnetic fields, the kink found in the in-plane magnetization between 2 and 3 T [Fig. 3(a)] marks the spin-flop reorientation field of the Néel vector into an in-plane direction orthogonal to the applied field. This is visible for any inplane direction since three equivalent easy axes exist in the basal plane [31]. First principle calculations let us also exclude the weak magnetization as source for the found AHE since significantly larger magnetization would be needed to yield a sizable AHE.

In Fig. 3(b) we show the conversion of ρ_{yx}^{AHE} at 175 and 300 K, and $\beta = 30°$ into the anomalous Hall conductivity $\sigma_{xy}^{\mathrm{AHE}}$. The temperature-dependent saturated and spontaneous AHE conductivity signals shown in Figs. 3(c) and 3(d) were extracted from $\sigma_{xy}^{\mathrm{AHE}}$ as indicated in Fig. 3(b). As expected for the AHE, they vanish when approaching the MnTe Néel temperature of 310 K. The complex temperature dependence below the Néel temperature can be governed by a combination of the variation of the longitudinal resistivity [30,41], the achievable degree of polarization of the system, as well as a potential variation of the Fermi level. Nevertheless the measured magnitude of $\sigma_{xy}^{\mathrm{AHE}}$ is within the scale predicted by our DFT calculations for the Fermi level on the order of ~20 meV below the valence-band edge, consistent with the hole density inferred from the ordinary Hall signal and using finite band broadening [41].

Finally, we note that hysteretic and spontaneous AHE signals are also found for the electrical current applied along the in-plane a axis ($[2\bar{1}\,\bar{1}\,0]$). This is consistent with the out-of-plane c-axis orientation of the AHE pseudo-vector that allows for the AHE detection with any in-plane applied current.

In conclusion, we have detected a spontaneous AHE in semiconducting MnTe with collinear compensated magnetic order. In magnetic field sweeps, we identify open and saturated hysteresis loops of the AHE signal, consistent with the $\mathcal{T}$-symmetry breaking by the antiparallel order of spins and anisotropic crystal environment in MnTe, and in contrast to the conventional AHE in ferromagnets generated by a macroscopic net magnetization. Our theoretical symmetry analysis and DFT calculations corroborate the experimental results. They confirm the favorable crystallographic orientation of the easy axis (axes) in MnTe films for generating the spontaneous AHE signal. DFT calculations of the intrinsic Berry-curvature contribution to the AHE conductivity are consistent with the measured scale of the AHE signals. Our Letter opens the prospect of exploring and exploiting $\mathcal{T}$-symmetry breaking phenomena arising from the unconventional altermagnetic phase in semiconductors and insulators.

---

[*]rhernandezj@uninorte.edu.co
[†]kriegner@fzu.cz

[1] N. Nagaosa, J. Sinova, S. Onoda, A. H. MacDonald, and N. P. Ong, Anomalous Hall effect, Rev. Mod. Phys. **82**, 1539 (2010).

[2] L. Šmejkal, A. H. MacDonald, J. Sinova, S. Nakatsuji, and T. Jungwirth, Anomalous Hall antiferromagnets, Nat. Rev. Mater. **7**, 482 (2022).

[3] L. Šmejkal, R. González-Hernández, T. Jungwirth, and J. Sinova, Crystal time-reversal symmetry breaking and spontaneous Hall effect in collinear antiferromagnets, Sci. Adv. **6**, eaaz8809 (2020).

[4] K. Samanta, M. Ležaić, M. Merte, F. Freimuth, S. Blügel, and Y. Mokrousov, Crystal Hall and crystal magneto-optical effect in thin films of $SrRuO_3$, J. Appl. Phys. **127**, 213904 (2020).

[5] M. Naka, S. Hayami, H. Kusunose, Y. Yanagi, Y. Motome, and H. Seo, Anomalous Hall effect in kappa-type organic antiferromagnets, Phys. Rev. B **102**, 075112 (2020).

[6] I. I. Mazin, K. Koepernik, M. D. Johannes, R. González-Hernández, and L. Šmejkal, Prediction of unconventional magnetism in doped $FeSb_2$, Proc. Natl. Acad. Sci. U.S.A. **118**, e2108924118 (2021).

[7] L. Šmejkal, J. Sinova, and T. Jungwirth, Beyond Conventional Ferromagnetism and Antiferromagnetism: A Phase with Nonrelativistic Spin and Crystal Rotation Symmetry, Phys. Rev. X **12**, 031042 (2022).

[8] L. Šmejkal, J. Sinova, and T. Jungwirth, Emerging research landscape of altermagnetism, arXiv:2204.10844.

[9] A. S. Núñez, R. A. Duine, P. Haney, and A. H. MacDonald, Theory of spin torques and giant magnetoresistance in antiferromagnetic metals, Phys. Rev. B **73**, 214426 (2006).

[10] L. Šmejkal, J. Železný, J. Sinova, and T. Jungwirth, Electric Control of Dirac Quasiparticles by Spin-Orbit Torque in an Antiferromagnet, Phys. Rev. Lett. **118**, 106402 (2017).

[11] T. Berlijn, P. C. Snijders, O. Delaire, H.-D. Zhou, T. A. Maier, H.-B. Cao, S.-X. Chi, M. Matsuda, Y. Wang, M. R. Koehler, P. R. C. Kent, and H. H. Weitering, Itinerant

Antiferromagnetism in RuO$_2$, Phys. Rev. Lett. **118**, 077201 (2017).

[12] Z. H. Zhu, J. Strempfer, R. R. Rao, C. A. Occhialini, J. Pelliciari, Y. Choi, T. Kawaguchi, H. You, J. F. Mitchell, Y. Shao-Horn, and R. Comin, Anomalous Antiferromagnetism in Metallic RuO$_2$ Determined by Resonant X-ray Scattering, Phys. Rev. Lett. **122**, 017202 (2019).

[13] Z. Feng, X. Zhou, L. Šmejkal, L. Wu, Z. Zhu, H. Guo, R. González-Hernández, X. Wang, H. Yan, P. Qin, X. Zhang, H. Wu, H. Chen, Z. Xia, C. Jiang, M. Coey, J. Sinova, T. Jungwirth, and Z. Liu, An anomalous Hall effect in altermagnetic ruthenium dioxide, Nat. Electron. **5**, 735 (2022).

[14] K.-H. Ahn, A. Hariki, K.-W. Lee, and J. Kuneš, Antiferromagnetism in RuO2 as d-wave Pomeranchuk instability, Phys. Rev. B **99**, 184432 (2019).

[15] S. Hayami, Y. Yanagi, and H. Kusunose, Momentum-dependent spin splitting by collinear antiferromagnetic ordering, J. Phys. Soc. Jpn. **88**, 123702 (2019).

[16] R. González-Hernández, L. Šmejkal, K. Výborný, Y. Yahagi, J. Sinova, T. Jungwirth, and J. Železný, Efficient Electrical Spin Splitter Based on Nonrelativistic Collinear Antiferromagnetism, Phys. Rev. Lett. **126**, 127701 (2021).

[17] L. Šmejkal, A. B. Hellenes, R. González-Hernández, J. Sinova, and T. Jungwirth, Giant and Tunneling Magnetoresistance in Unconventional Collinear Antiferromagnets with Nonrelativistic Spin-Momentum Coupling, Phys. Rev. X **12**, 011028 (2022).

[18] D.-F. Shao, S.-H. Zhang, M. Li, C.-B. Eom, and E. Y. Tsymbal, Spin-neutral currents for spintronics, Nat. Commun. **12**, 7061 (2021).

[19] A. Bose, N. J. Schreiber, R. Jain, D.-F. Shao, H. P. Nair, J. Sun, X. S. Zhang, D. A. Muller, E. Y. Tsymbal, D. G. Schlom, and D. C. Ralph, Tilted spin current generated by the collinear antiferromagnet ruthenium dioxide, Nat. Electron. **5**, 267 (2022).

[20] H. Bai, L. Han, X. Y. Feng, Y. J. Zhou, R. X. Su, Q. Wang, L. Y. Liao, W. X. Zhu, X. Z. Chen, F. Pan, X. L. Fan, and C. Song, Observation of Spin Splitting Torque in a Collinear Antiferromagnet RuO$_2$, Phys. Rev. Lett. **128**, 197202 (2022).

[21] S. Karube, T. Tanaka, D. Sugawara, N. Kadoguchi, M. Kohda, and J. Nitta, Observation of Spin-Splitter Torque in Collinear Antiferromagnetic RuO$_2$, Phys. Rev. Lett. **129**, 137201 (2022).

[22] D. Kriegner, K. Výborný, K. Olejník, H. Reichlová, V. Novák, X. Marti, J. Gazquez, V. Saidl, P. Němec, V. V. Volobuev, G. Springholz, V. Holý, and T. Jungwirth, Multiple-stable anisotropic magnetoresistance memory in antiferromagnetic MnTe, Nat. Commun. **7**, 11623 (2016).

[23] S. Greenwald, The antiferromagnetic structure deformations in CoO and MnTe, Acta Crystallogr. **6**, 396 (1953).

[24] T. Komatsubara, M. Murakami, and E. Hirahara, Magnetic properties of manganese telluride single crystals, J. Phys. Soc. Jpn. **18**, 356 (1963).

[25] N. Kunitomi, Y. Hamaguchi, and S. Anzai, Neutron diffraction study on manganese telluride, J. Phys. (Les Ulis, Fr.) **25**, 568 (1964).

[26] J. W. Allen, G. Lucovsky, and J. C. Mikkelsen, Optical properties and electronic structure of crossroads material MnTe, Solid State Commun. **24**, 367 (1977).

[27] M. Podgorny and J. Oleszkiewicz, Electronic structure of antiferromagnetic MnTe, J. Phys. C **16**, 2547 (1983).

[28] S.-H. Wei and A. Zunger, Total-energy and band-structure calculations for the semimagnetic Cd1-xMnxTe semiconductor alloy and its binary constituents, Phys. Rev. B **35**, 2340 (1987).

[29] E. Przeździecka, E. Kamińska, E. Dynowska, R. Butkutė, W. Dobrowolski, H. Kępa, R. Jakiela, M. Aleszkiewicz, E. Łusakowska, E. Janik, and J. Kossut, Preparation and characterization of hexagonal MnTe and ZnO layers, Phys. Status Solidi C **2**, 1218 (2005).

[30] Y. Magnin and H. T. Diep, Monte Carlo study of magnetic resistivity in semiconducting MnTe, Phys. Rev. B **85**, 184413 (2012).

[31] D. Kriegner, H. Reichlova, J. Grenzer, W. Schmidt, E. Ressouche, J. Godinho, T. Wagner, S. Y. Martin, A. B. Shick, V. V. Volobuev, G. Springholz, V. Holý, J. Wunderlich, T. Jungwirth, and K. Výborný, Magnetic anisotropy in antiferromagnetic hexagonal MnTe, Phys. Rev. B **96**, 214418 (2017).

[32] G. Yin, J.-X. Yu, Y. Liu, R. K. Lake, J. Zang, and K. L. Wang, Planar Hall Effect in Antiferromagnetic MnTe Thin Films, Phys. Rev. Lett. **122**, 106602 (2019).

[33] S. Mu, R. P. Hermann, S. Gorsse, H. Zhao, M. E. Manley, R. S. Fishman, and L. Lindsay, Phonons, magnons, and lattice thermal transport in antiferromagnetic semiconductor MnTe, Phys. Rev. Mater. **3**, 025403 (2019).

[34] D. Bossini, S. Dal Conte, M. Terschanski, G. Springholz, A. Bonanni, K. Deltenre, F. Anders, G. S. Uhrig, G. Cerullo, and M. Cinchetti, Femtosecond phononic coupling to both spins and charges in a room-temperature antiferromagnetic semiconductor, Phys. Rev. B **104**, 224424 (2021).

[35] G. Zanmarchi, Optical measurements on the antiferromagnetic semiconductor MnTe, J. Phys. Chem. Solids **28**, 2123 (1967).

[36] C. Ferrer-Roca, A. Segura, C. Reig, and V. Muñoz, Temperature and pressure dependence of the optical absorption in hexagonal MnTe, Phys. Rev. B **61**, 13679 (2000).

[37] H. Ohno, Making nonmagnetic semiconductors ferromagnetic, Science **281**, 951 (1998).

[38] T. Dietl and H. Ohno, Dilute ferromagnetic semiconductors: Physics and spintronic structures, Rev. Mod. Phys. **86**, 187 (2014).

[39] T. Jungwirth, J. Wunderlich, V. Novák, K. Olejník, B. L. Gallagher, R. P. Campion, K. W. Edmonds, A. W. Rushforth, A. J. Ferguson, and P. Němec, Spin-dependent phenomena and device concepts explored in (Ga,Mn)As, Rev. Mod. Phys. **86**, 855 (2014).

[40] P. Villars and K. Cenzual, MnTe Crystal Structure: Datasheet from "PAULING FILE Multinaries Edition—2012" in *SpringerMaterials* (Springer-Verlag Berlin Heidelberg & Material Phases Data System (MPDS), Switzerland & National Institute for Materials Science (NIMS), Japan, 2016), https://materials.springer.com/isp/crystallographic/docs/sd_0379437.

[41] See Supplemental Material at http://link.aps.org/supplemental/10.1103/PhysRevLett.130.036702 for additional experimental data and figures, which includes Refs. [42–49].

[42] G. Kresse and J. Furthmüller, Efficient iterative schemes for ab initio total-energy calculations using a plane-wave basis set, Phys. Rev. B **54**, 11169 (1996).

[43] A. A. Mostofi, J. R. Yates, G. Pizzi, Y.-S. Lee, I. Souza, D. Vanderbilt, and N. Marzari, An updated version of Wannier90: A tool for obtaining maximally-localised Wannier functions, Comput. Phys. Commun. **185**, 2309 (2014).

[44] G. Pizzi *et al.*, Wannier90 as a community code: New features and applications, J. Phys. Condens. Matter **32**, 165902 (2020).

[45] Q. Wu, S. Zhang, H.-F. Song, M. Troyer, and A. A. Soluyanov, WannierTools: An open-source software package for novel topological materials, Comput. Phys. Commun. **224**, 405 (2018).

[46] F. Freimuth, S. Blügel, and Y. Mokrousov, Spin-orbit torques in Co/Pt(111) and Mn/W(001) magnetic bilayers from first principles, Phys. Rev. B **90**, 174423 (2014).

[47] J. Železný, https://bitbucket.org/zeleznyj/wannier-linear-response.

[48] J. Železný, https://bitbucket.org/zeleznyj/linear-response-symmetry.

[49] E. D. Ranieri, A. W. Rushforth, K. Výborný, U. Rana, E. Ahmad, R. P. Campion, C. T. Foxon, B. L. Gallagher, A. C. Irvine, J. Wunderlich, and T. Jungwirth, Lithographically and electrically controlled strain effects on anisotropic magnetoresistance in (Ga,Mn)As, New J. Phys. **10**, 065003 (2008).

[50] Note that we use Bravais indices $hkil$, with $i = -h - k$ for the hexagonal MnTe, while Miller indices hkl are used for the cubic substrate.

[51] J. Wasscher, Electrical transport phenomena in MnTe, an antiferromagnetic semiconductor, Ph.D. thesis, Technische Hogeschool Eindhoven, 1969, 10.6100/IR43336.

[52] L. Landau and E. Lifshitz, *Electrodynamics of Continuous Media, Vol. 8 of Course of Theoretical Physics* 2nd ed. (Pergamon Press, Oxford, 1984).